Supplementary information

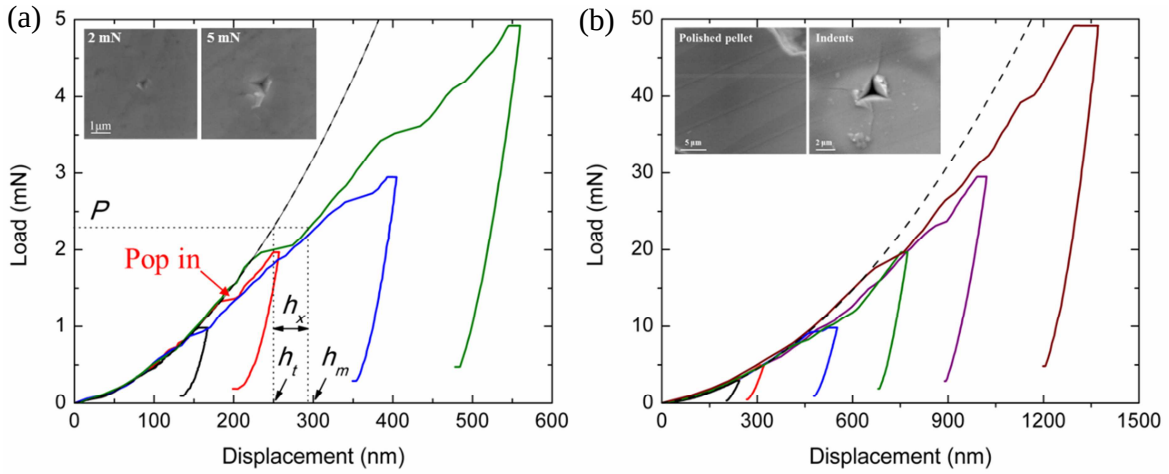

Figure S1. Load-displacement responses of (a) NMC secondary particles and (b) NMC pellets under different indentation loads using cube corner indenter. NMC pellets show a much higher cracking threshold than the NMC secondary particles. The inset SEM images show the indentation impression under different loads.

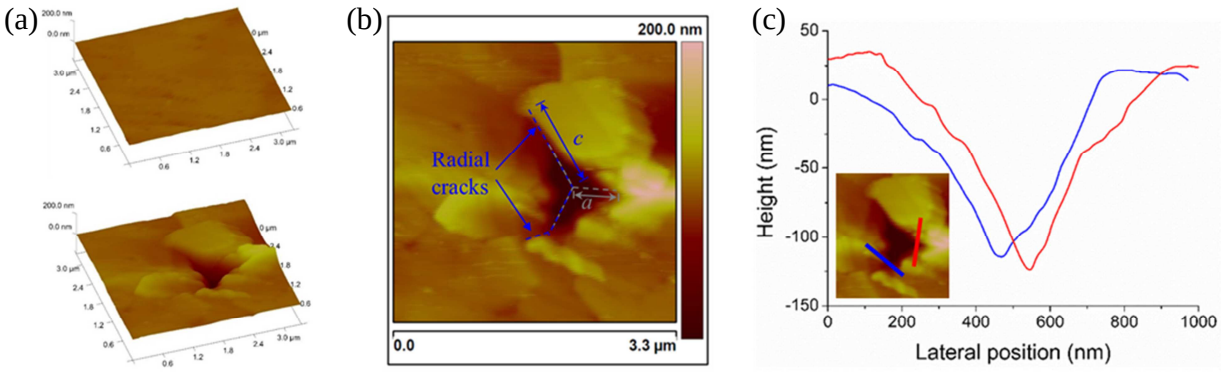

Figure S2. AFM images showing (a) the surface morphologies of NMC particles before and after nanoindentation, (b) the indentation impression and the radial cracks, and (c) surface invagination and cracking caused by indentation. The red and blue lines in the inset of (c) represent the locations in the height scanning profiles.

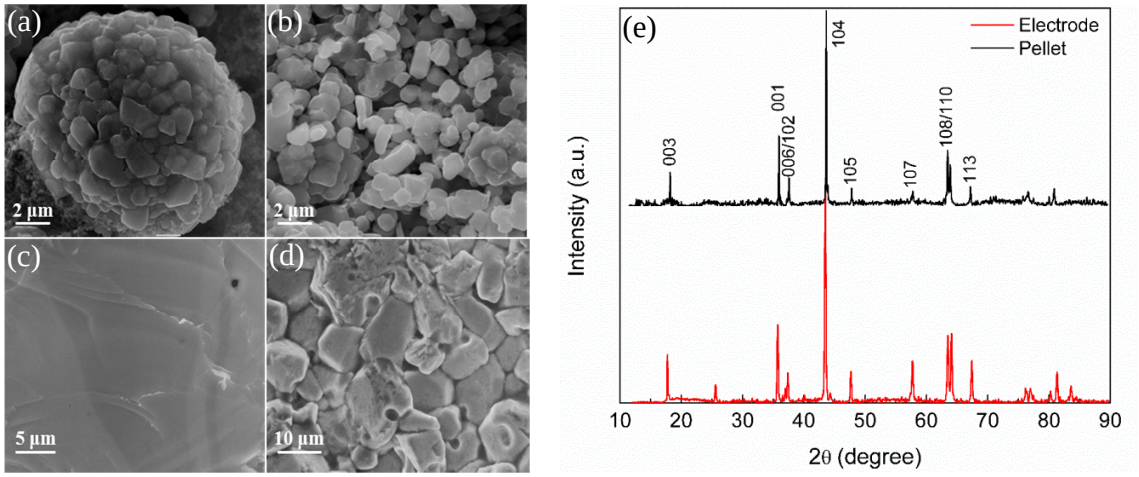

Figure S3. SEM images of (a) a NMC secondary particle, (b) NMC primary particles, (c) surface of the sintered NMC pellet, (d) fractured surface of sintered NMC pellet. (e) XRD profiles of NMC electrode and sintered pellets. The additional peak at 2θ = 26.8° for NMC electrode is induced by the carbon black contained in the electrode. The XRD patterns show that the NMC particles in electrode and pellets have the same chemical compositions.

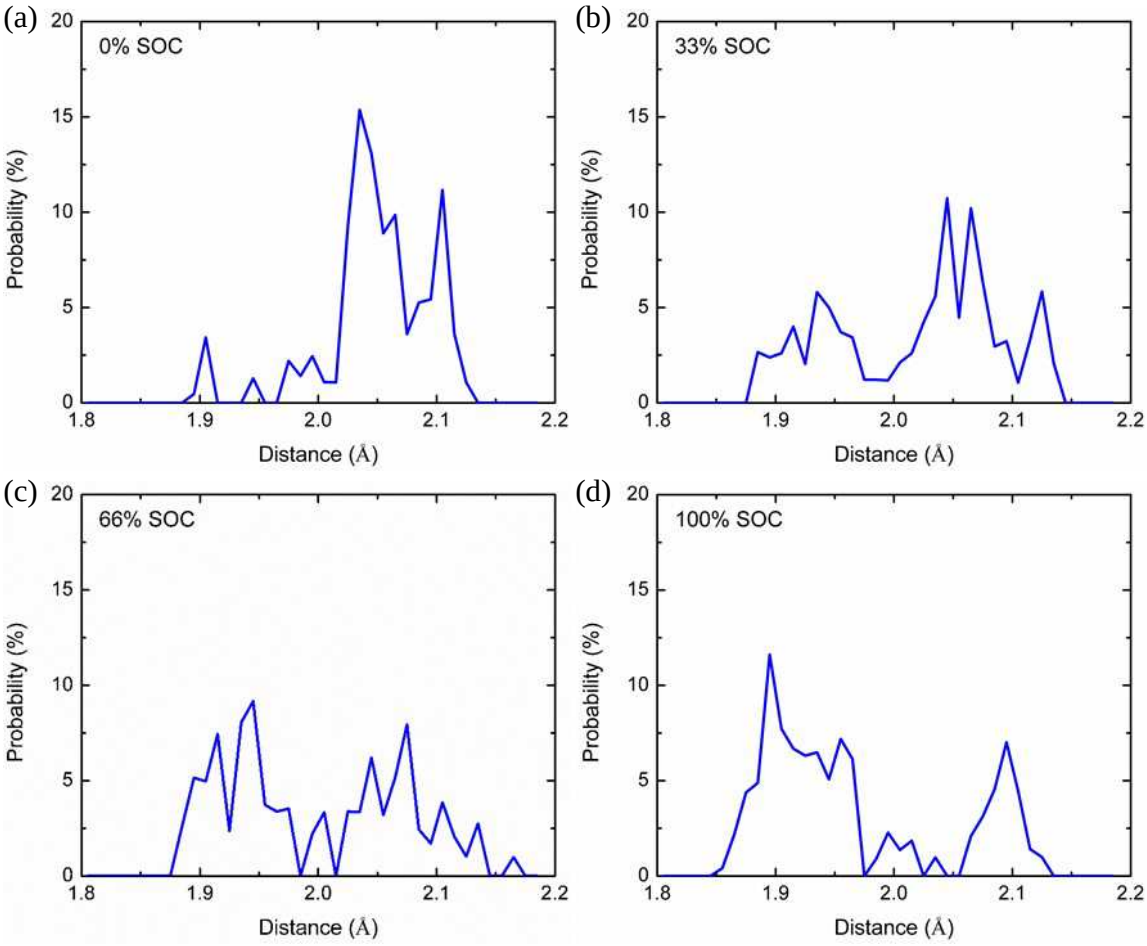

Figure S4. The Ni-O bond length distribution in NMC at different states of charge. During delithiation, the Ni-O bond length decreases implying the transition from Ni^{2+} into Ni^{3+}.

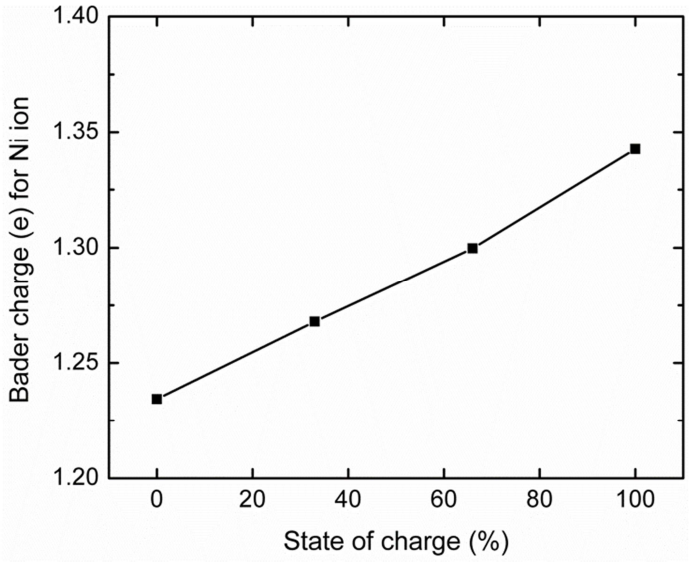

Figure S5. The gradual increase of Bader charge of Ni during delithiation.

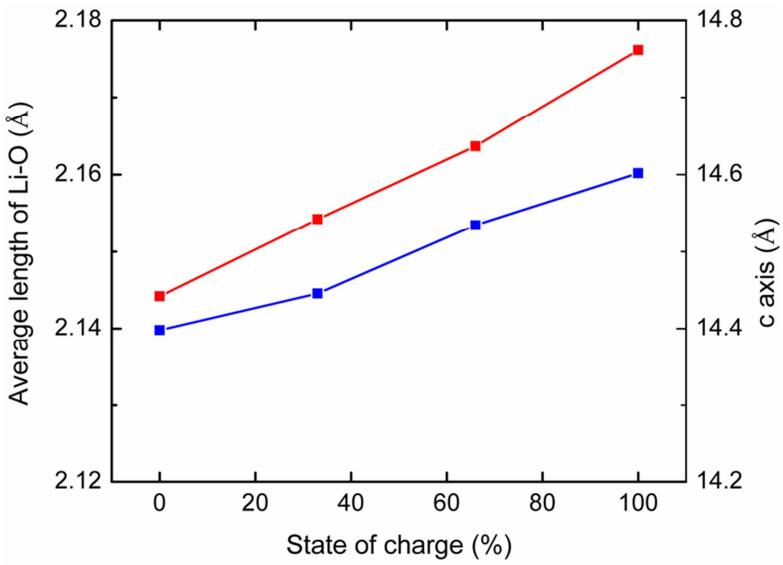

Figure S6. The gradual increase of Li-O bond length and *c*-axis lattice parameter during delithiation of NMC.

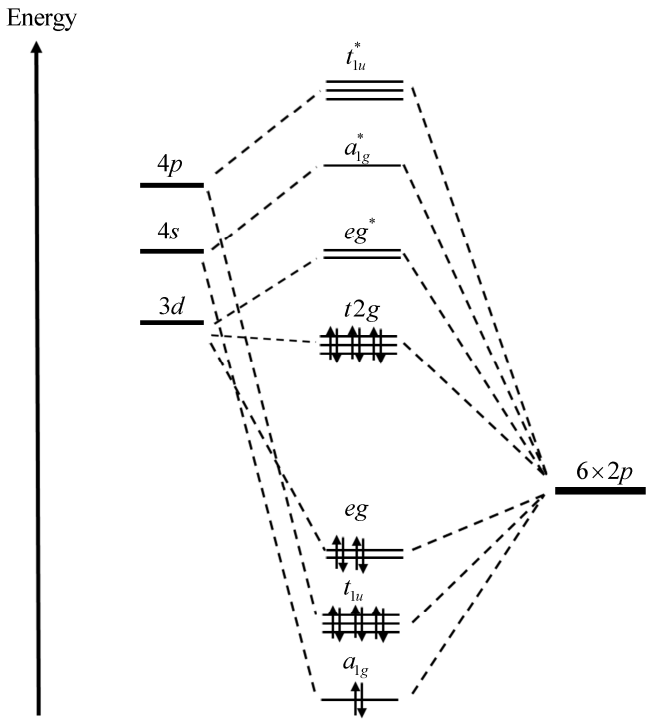

Figure S7. Molecular orbital diagram of the transition metal complex showing the *d* orbital electron population of Co^{3+} and O 2*p* orbital.